

Probing solar-cycle variations of magnetic fields in the convection zone using meridional flows

Chia-Hsien Lin¹  and Dean-Yi Chou²

¹Graduate Institute of Space Science, National Central University, Taiwan
email: chlin@jupiter.ss.ncu.edu.tw

²Department of Physics, National Tsing-Hua University, Taiwan
email: chou@phys.nthu.edu.tw

Abstract. Solar magnetic fields are believed to originate from the base of convection zone. However, it has been difficult to obtain convincing observational evidence of the magnetic fields in the deep convection zone. The goal of this study is to investigate whether solar meridional flows can be used to detect the magnetic-field effects. Meridional flows are axisymmetric flows on the meridional plane. Our result shows that the flow pattern in the entire convection zone changes significantly from solar minimum to maximum. The changes all centered around active latitudes, suggesting that the magnetic fields are responsible for the changes. The results indicate that the meridional flow can be used to detect the effects of magnetic field in the deep convection zone.

The results have been published in the *Astrophysical Journal* (Lin & Chou 2018).

Keywords. Sun: helioseismology, Sun: magnetic fields, Sun: oscillations

1. Introduction

The solar magnetic fields are the main driver for most of observed solar activities and phenomena. However, how and where they are generated are still not fully understood. While it is generally accepted that they are generated by a dynamo mechanism at the base of the convection zone and brought up by magnetic buoyancy, there has been no unambiguous observational evidence for the existence of magnetic field in the deep convection zone. It is because the effects of the magnetic fields on the properties of waves are too weak to be distinguished from noise by current observation and analysis capability.

Solar meridional flows are axisymmetric flows on the meridional planes, and penetrate the entire convection zone. They play an important role in transporting magnetic flux and energy, and can, in turn, be affected by the magnetic fields. Liang & Chou (2015) applied the time-distance analysis method (see, e.g., Kosovichev 1996, Giles 1999, Zhao & Kosovichev 2004) to examine the solar-cycle variation of the travel-time difference of waves due to the meridional flow in the convection zone. Their results show that the pattern of the travel-time difference changes with solar cycle. This indicates that the meridional flows are sensitive to the variation in the solar magnetic activity. In this study, we apply a helioseismic inversion procedure to the travel-time difference data from Liang & Chou (2015) to infer the meridional flow patterns during the solar minimum and maximum, and examine whether the difference in the patterns are related to the magnetic fields.

2. Travel-time difference Data

Liang & Chou (2015) used the full-disk Doppler images taken by Michelson Doppler Imager (MDI) on board Solar and Heliospheric Observatory (SOHO) spacecraft (Scherrer *et al.* 1995) to measure the travel-time difference $\delta\tau$ of different travel distances Δ_n , at different latitudes L_m , and at different times t from May 1996 to November 2010, which includes two solar minima and one maximum. To reduce the error caused by telescope pointing, they kept only the anti-symmetric component of $\delta\tau$ relative to the equator. Their results indicate that the patterns of the travel-time difference of the two minima are similar, but are significantly different from that of the maximum.

In this study, we averaged their measured $\delta\tau(L_m, \Delta_n, t)$ over the two minimum periods (May 1996 to December 1997, and January 2008 to December 2009) to represent the travel-time difference of the solar minimum, $\delta\tau^{(\min)}(L_m, \Delta_n)$, and averaged the travel-time difference over the one maximum period (January 2000 to December 2001) to represent the travel-time difference for the solar maximum, $\delta\tau^{(\max)}(L_m, \Delta_n)$. The travel-time difference data used for this study are shown in Fig. 1 (adapted from Lin & Chou 2018). The panels (A), (C), and (E) are the patterns of $\delta\tau^{(\min)}$, $\delta\tau^{(\max)}$, and the difference between the two $\delta\tau^{(\text{diff})} = \delta\tau^{(\max)} - \delta\tau^{(\min)}$. Positive $\delta\tau$ corresponds to northward flow, and vice versa. Their respective errors are shown in panels (B), (D), and (F). The exact ranges of the travel distances and the latitude locations used in our study to estimate the meridional flow are 89 travel distances in the range $7.2^\circ \leq \Delta_n \leq 60^\circ$, and 79 latitudes in the range $-39^\circ \leq L_m \leq 39^\circ$ for the shallowest layer.

3. Inversion methods

In this study, the travel-time difference is related to the meridional flow by the ray path approximation, which assumes that the propagation of acoustic waves can be represented by their ray paths. Although the measured $\delta\tau$ consists of the contributions from the horizontal and radial components of the meridional flow, Giles (1999) showed that the contribution from the radial flow component is much smaller than the contribution from the horizontal flow component. Therefore, we neglected the radial flow contribution to $\delta\tau$ (Kosovichev 1996, Giles 1999, Kosovichev *et al.* 2000):

$$\delta\tau(L_m, \Delta_n) = -2 \int_{\Gamma(L_m, \Delta_n)} \frac{\mathbf{U} \cdot \mathbf{n}}{c^2} ds \quad (3.1)$$

$$\approx \int_{\Gamma(L_m, \Delta_n)} \frac{V_{\text{gh}}}{c^2 V_{\text{gr}}} U_h ds, \quad (3.2)$$

$$\approx \sum_{i,j} K(L_m, \Delta_n; r_i, \theta_j) U_h(r_i, \theta_j), \quad (3.3)$$

where c is the sound speed, \mathbf{U} is the flow velocity, \mathbf{n} is the unit vector along the ray path Γ , which is specified by L_m and Δ_n , U_h is the horizontal (latitudinal) component of the flow velocity, and V_{gh} and V_{gr} are the horizontal and radial components of the group velocity of the acoustic wave, respectively. The last equation is the discretized form of the integration, where r_i and θ_j are the radial and latitudinal coordinates of the grid points, and K is called the sensitivity kernel and can be computed from the standard solar model of Christensen-Dalsgaard *et al.* (1996).

To determine U_h , we implemented the Subtractive Optimally Localized Averages (SOLA) inversion method (Pijpers & Thompson 1994). The basic idea of SOLA is to superpose the sensitivity kernels corresponding to different ray paths to form a localized averaging kernel around a target point $(r_{i'}, \theta_{j'})$. The weighting coefficients C_{mn} of the

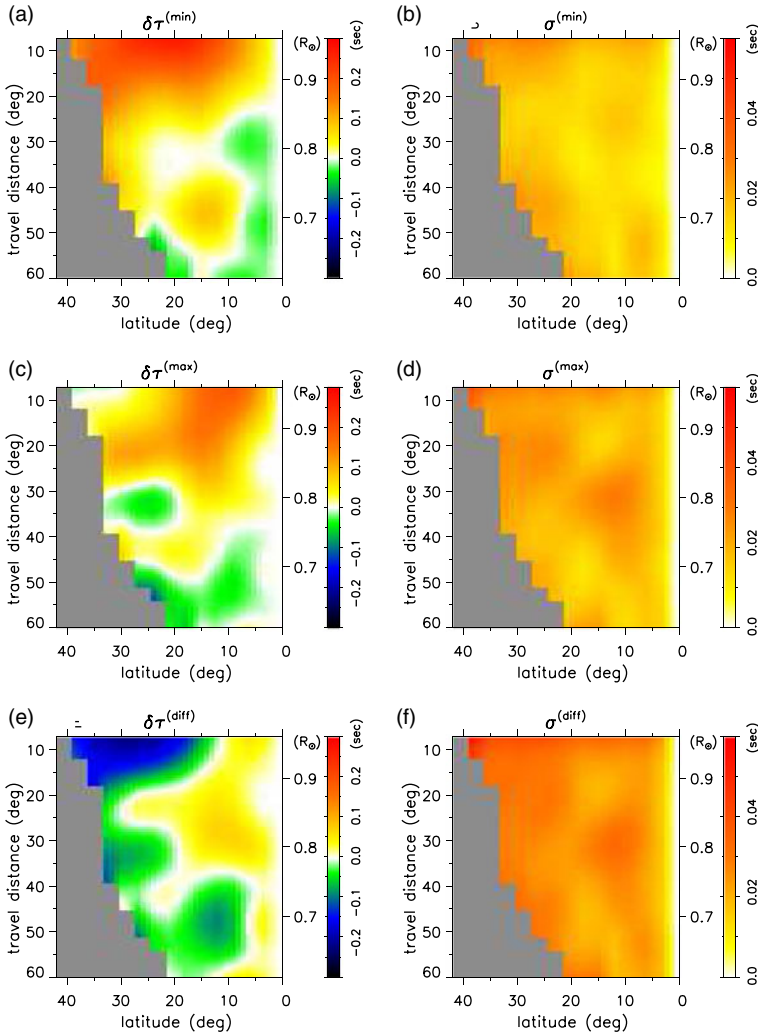


Figure 1. Measured travel-time difference at the solar minimum (panel A), solar maximum (panel C), and their difference (panel E). The three right panels are the corresponding measurement errors. The left- and right-side axis labels of each panel are the travel distance and the corresponding radius of the lower turning point, respectively.

superposition is determined by minimizing the difference between the averaging kernel and a target function which peaks at the target point and small else where:

$$\sum_{mn} C_{mn}^{i'j'} \delta\tau(L_m, \Delta_n) = \sum_{mn} \sum_{ij} C_{mn}^{i'j'} K(L_m, \Delta_n; r_i, \theta_j) U_h(r_i, \theta_j) + \sum_{mn} C_{mn}^{i'j'} \sigma_{mn} \tag{3.4}$$

$$\approx \sum_{ij} \bar{K}^{i'j'}(r_i, \theta_j) U_h(r_i, \theta_j) \tag{3.5}$$

$$\approx \sum_{ij} T^{i'j'}(r_i, \theta_j) U_h(r_i, \theta_j) \tag{3.6}$$

$$\approx \langle U_h \rangle_{i'j'} \tag{3.7}$$

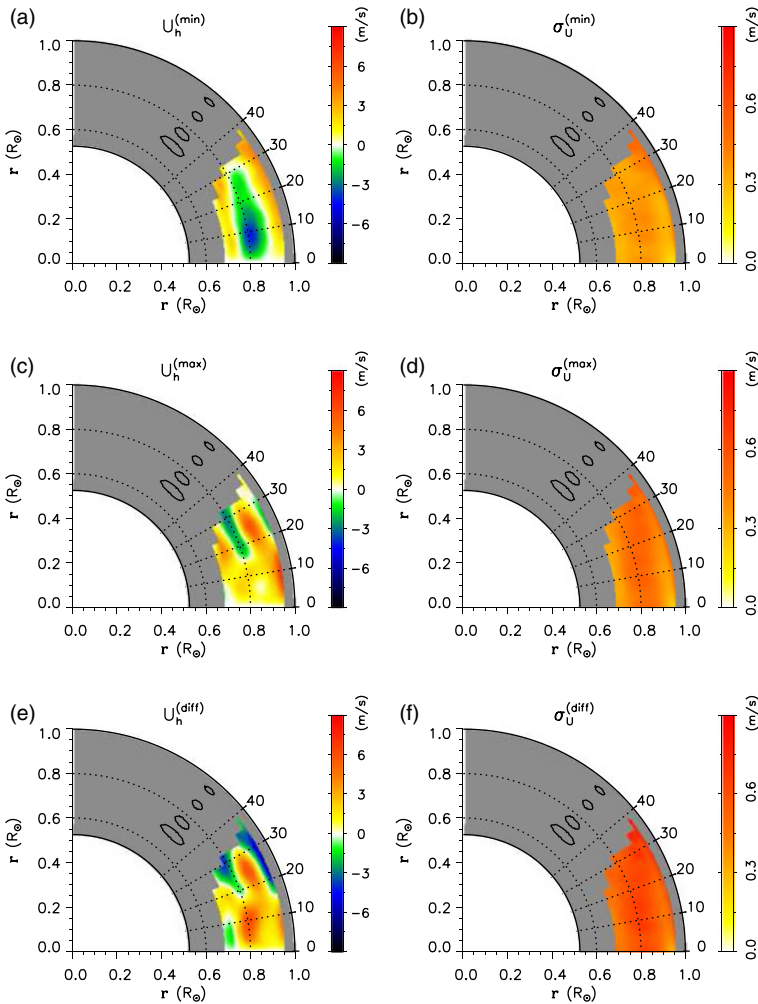


Figure 2. Estimated horizontal component of the meridional flow at the minimum (panel A), maximum (panel C), and their difference (panel E). The three right panels show the corresponding errors. The contours represent the half-maximum widths of the averaging kernels at four different depths.

where the superscripts i' and j' correspond to the subscripts of target point $(r_{i'}, \theta_{j'})$, σ_{mn} is the measurement error of travel-time difference, $\bar{K}^{i'j'}$ and $T^{i'j'}$ are the averaging kernel and the target function of the target point (i', j') , respectively, and $\langle U_h \rangle_{i'j'}$ is an estimate of U_h from the inversion with an estimated error of $\sqrt{\sum_{mn} (C_{mn}^{i'j'} \sigma_{mn})^2}$. To compute $\{C_{mn}^{i'j'}\}$, we applied the Singular Value Decomposition (SVD) method (Press *et al.* 1992).

4. Results and discussion

The inversion results using measured $\delta\tau(L_m, \Delta_n)$ are shown in Fig. 2 (adapted from Lin & Chou 2018). Panels (A), (C) and (E) show the horizontal flow speed at the minimum, $U_h^{(\min)}$, maximum, $U_h^{(\max)}$, and the difference between the two, $U_h^{(\text{diff})}$, respectively. The three right panels (B), (D) and (F) are their corresponding errors. The half-maximum

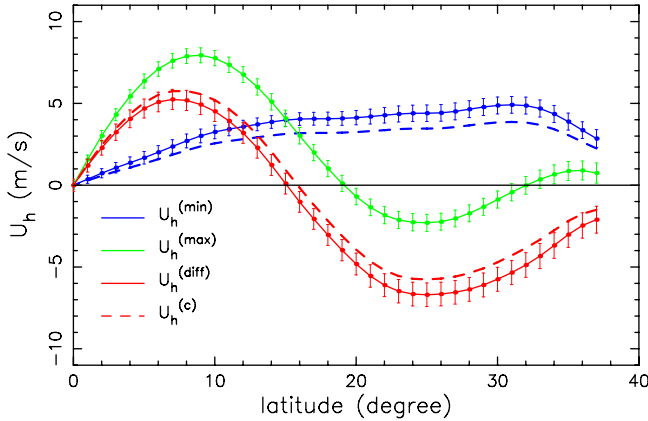


Figure 3. Estimated horizontal flow at $0.96R_{\odot}$ for the minimum (blue solid line), the maximum (green solid line), and their difference (red solid line). The blue dashed line is $\alpha U_h^{(\min)}$ using $\alpha = 0.79$, and the red dashed line is the resulting $U_h^{(c)}$, computed from Equation (4.1).

widths of the averaging kernels at four different depths are represented by the contours in the high-latitude gray area where no data are available.

The figure shows that the flow pattern in the entire convection zone changes significantly from solar minimum to maximum. Panel (A) shows that during the minimum, the horizontal flow has a three-layer structure in $0.67 \leq r \leq 0.96R_{\odot}$: a poleward flow in the upper convection zone, an equator-ward in the middle convection zone, and a poleward flow again in the lower convection zone. The flow speed is close to zero within the error bar around the base of the convection zone, located at $0.7R_{\odot}$. This three-layer structure is similar to the result of [Chen & Zhao \(2017\)](#), which uses the HMI data in the period of 2010.05 – 2017.04, cycle 24. The difference between the maximum and minimum can be seen clearly in panel (E). It shows that the most prominent changes from the minimum to maximum flow are the appearance of a convergent flow above $0.9R_{\odot}$, another around $0.8R_{\odot}$, and a weak divergent flow near the base of convection zone. The signal-to-noise ratio of this weak divergent flow is about 3–4. It is interesting to note that all these changes are centered around the active latitudes $\approx 15 - 17^{\circ}$.

To compare our results with the direct measurements of the surface meridional flow by previous studies, we plotted the the result of our shallowest layer ($0.96R_{\odot}$) in Fig. 3 (adapted from [Lin & Chou 2018](#)). The latitudinal dependence of $U_h^{(\min)}$ (blue solid line) is similar to the typical sine-shape distribution, but $U_h^{(\max)}$ (green solid line) is significantly different from $U_h^{(\min)}$. The difference $U_h^{(\text{diff})}$ (red solid line) changes sign at the active latitude $\approx 15^{\circ}$ ([Liang & Chou 2015](#)). The pattern of $U_h^{(\text{diff})}$ indicates that at the solar maximum, an additional convergent flow toward the active latitudes is generated relative to the flow at the solar minimum. To approximate the pattern of $U_h^{(\max)}$, we can combine a reduced $U_h^{(\min)}$ and a convergent flow:

$$U_h^{(\max)}(L) = \alpha U_h^{(\min)}(L) + U_h^{(c)}(L), \quad (4.1)$$

where α is the suppression coefficient describing the reduction in flow magnitude, and $U_h^{(c)}(L)$ is the the convergent flow. With the simplification assumptions that α is a constant and the peaks of $|U_h^{(c)}(L)|$ above and below the active latitude are equal, we determined the value of α to be 0.79 using measured $U_h^{(\min)}(L)$ and $U_h^{(\max)}(L)$. The blue dashed line in Fig. 3 represents $\alpha U_h^{(\min)}(L)$ using $\alpha = 0.79$, and the resulting $U_h^{(c)}(L)$ is

plotted as the red dashed line. $U_h^{(c)}(L)$ is approximately anti-symmetric with respect to latitude 16° , with a peak speed of 5.8 m s^{-1} at about 7° and 25° .

Earlier study by Hathaway & Rightmire (2010) reported a reduction of about 30% in flow speed at the maximum on the surface. In comparison, our analysis suggests a reduction of about 21% at $0.96R_\odot$. The convergent flow around the active latitudes at the maximum has also been reported in previous studies. Hathaway & Rightmire (2011) reported a convergent flow of about several m s^{-1} on the surface at the maximum. The time-distance analysis by Zhao & Kosovichev (2004) reported a magnitude of the convergent flow about $2 - 8 \text{ m s}^{-1}$ at $0.987R_\odot - 0.996R_\odot$. The ring-diagram analysis by Haber *et al.* (2002) obtained a magnitude of about several m s^{-1} at $0.99R_\odot$. In our study, the magnitude of the convergent flow is 5.8 m s^{-1} at $0.96R_\odot$.

5. Conclusion

The objective of this study is to investigate the solar-cycle variation of the meridional flow and whether the variation can be used to probe the magnetic fields.

The results show that the horizontal flow during minimum has three layers: a poleward flow in the upper and lower convection zone, and an equator-ward flow in the middle convection zone. The flow changes significantly from the minimum to maximum. The main differences are the reduction in flow magnitude and the appearance of two convergent flows and a weak divergent flow at the maximum. The convergent flows and the divergent flow are all centered around the active latitudes, suggesting that the changes are related to the magnetic fields. The results indicate that the solar-cycle variation of the meridional flow can be used to probe the magnetic fields in the deep convection zone.

References

- Chen, R. & Zhao, J. 2017, *ApJ*, 849, 144
 Christensen-Dalsgaard, J., Dappen, W., Ajukov, S. V., *et al.* 1996, *Science*, 272, 1286
 Giles, P. M. 1999, *PhD thesis, Stanford Univ.*
 Haber, D. A., Hindman, B. W., Toomre, J., Bogart, R., & Larsen, R. 2002 *ApJ*, 570, 855
 Hathaway, D. H. & Rightmire, L. 2010, *Science*, 327, 1350
 Hathaway, D. H. & Rightmire, L. 2011, *ApJ*, 729, 80
 Kosovichev, A. G. 1996, *ApJL*, 461, L55
 Kosovichev, A. G., Duvall, T. J., Jr., & Scherrer, P. H. 2000 *SoPh*, 192, 159
 Liang, Z.-C. & Chou, D.-Y. 2015, *ApJ*, 809, 150
 Lin, C.-H. & Chou, D.-Y. 2018, *ApJ*, 860, 48
 Pijpers, F. P. & Thompson, M. J. 1994, *A&A*, 281, 231
 Press, W. H., Teukolsky, S. A., Vetterling, W. T., & Flannery, B. P. 1992, *Numerical Recipes in C (2nd ed.): The Art of Scientific Computing (New York: Cambridge Univ. Press)*
 Scherrer, P. H., Bogart, R. S., Bush, R. I., *et al.* 1995, *SoPh*, 162, 129
 Zhao, J. & Kosovichev, A. G. 2004, *ApJ*, 603, 776

Discussion

ALEXANDER KOSOVICHEV ASKED: Did you find a N-S asymmetry of the meridional flow?

CHIA-HSIEN LIN REPLIED: There is no asymmetric information in the data because only the anti-symmetric component is kept.

IRINA KITIASHVILI ASKED: How does meridional flow speed vary with solar cycle?

CHIA-HSIEN LIN REPLIED: The meridional flow has a 3-layer pattern during minimum, and becomes more complicated during the maximum.